First-in-class allosteric inhibitors of bacterial IMPDHs

Thomas Alexandre, Alexandru Lupan, Olivier Helynck, Sophie Vichier-Guerre, Laurence Dugué, Muriel Gelin, Ahmed Haouz, Gilles Labesse, Hélène Munier-Lehmann

First-in-class allosteric inhibitors of bacterial IMPDHs

Thomas Alexandre[1,2]‡, Alexandru Lupan[1§], Olivier Helynck[1]
Sophie Vichier-Guerre[1], Laurence Dugué[1], Muriel Gelin[3,4], Ahmed Haouz[5], Gilles Labesse*[3,4], Hélène Munier-Lehmann[1]*

[1]Institut Pasteur, Unité de Chimie et Biocatalyse, Département de Biologie Structurale et Chimie, CNRS UMR3523, 28 rue du Dr Roux, F-75015 Paris, France

[2]Université Paris Diderot, Sorbonne Paris Cité, F-75205 Paris, France

[3]CNRS, UMR5048, Université Montpellier; Centre de Biochimie Structurale, 29 rue de Navacelles, F-34090 Montpellier, France

[4]INSERM, U1054; Centre de Biochimie Structurale, F-34090 Montpellier, France

[5]Institut Pasteur, Plate-Forme de Cristallographie, CNRS UMR3528, F-75015 Paris, France

‡ Present address: Department of Microbiology and Immunobiology, Harvard Medical School, Boston, MA 02115, USA.

§ Present address: Faculty of Chemistry and Chemical Engineering, Babes-Bolyai University, Cluj-Napoca, Romania

*To whom correspondance should be addressed:
e-mail: labesse@cbs.cnrs.fr or helene.munier-lehmann@pasteur.fr

Keywords: nucleotide metabolism; chemical library screening; quaternary structure;

Bateman domain; allosteric inhibitor; IMPDH

ABSTRACT

Inosine-5'-monophosphate dehydrogenase (IMPDH) is an essential enzyme in many bacterial pathogens and is considered as a potential drug target for the development of new antibacterial agents. Our recent work has revealed the crucial role of one of the two structural domains (i.e. Bateman domain) in the regulation of the quaternary structure and enzymatic activity of bacterial IMPDHs. Thus, we have screened chemical libraries to search for compounds targeting the Bateman domain and identified first in-class allosteric inhibitors of a bacterial IMPDH. These inhibitors were shown to counteract the activation by the natural positive effector, MgATP, and to block the enzyme in its apo conformation (low affinity for IMP). Our structural studies demonstrate the versatility of the Bateman domain to accommodate totally unrelated chemical scaffolds and pave the way for the development of allosteric inhibitors, an avenue little explored until now.

1. Introduction

The Bateman domain was first identified by sequence analysis of a wide range of proteins [1]. It contains a tandem of 60-residue long domains called CBS domains, CBS standing for cystathionine β-synthase. According to the sole crystal structure available at that time, namely the one of inosine-5'-monophosphate dehydrogenase (IMPDH) [2], each CBS domain is composed of three β-strands and three α-helices. The function and putative ligands of Bateman domains remained for a long time unknown. Since then, it was shown that most Bateman domains are able to dimerize and bind adenosine-containing ligands at their dimerization interface [3]. So far, these ligands are AMP, ADP, ATP, S-adenosyl methionine (SAM) or NAD and they act as allosteric effectors. These domains are involved in the regulation of the function of numerous proteins and are the loci of mutations leading to human hereditary diseases [4, 5].

In human cystathionine β-synthase, the Bateman domains, located at the C-terminal part of the protein, are involved in tetramer stabilization [6] and enzymatic activity modulation [7]. They are autoinhibitory domains, whose effect is alleviated through the Bateman domain removal or SAM binding. In AMP activated kinase protein, the γ-subunit is composed of two Bateman domains. This subunit is responsible for a complex allosteric regulation upon ATP/ADP/AMP binding, with AMP and ATP having dual and opposite effects [8]. On the other hand, ATP/ADP/AMP binding to the Bateman domain of two human chloride ions channels (CLC-1 and CLC-5) leads to the same effects in the CLCs gating [9]. However, these effects are opposite depending on the channel type: nucleotide binding potentiates CLC-5 currents, whereas it inhibits the CLC-1 transporter.

IMPDH is another example of a protein containing a Bateman domain, which is, at the primary sequence level, inserted within the catalytic domain. This ubiquitous enzyme

converts IMP to xanthine-5'-monophosphate (XMP) using NAD^+ as a cofactor in the presence of water. As IMP is at a metabolic crossroad between guanine and adenine nucleotides biosynthesis pathways, human IMPDHs have emerged as major targets for drug development [10, 11]. The most well-known IMPDH inhibitors are NAD mimics derived from mycophenolic acid (MPA [12]) and the processed prodrug tiazofurin [13] used for immunosuppressive and anticancer therapy, respectively. Ribavirin, an antiviral drug, is competing for IMP [10, 11]. All these compounds bind to the IMPDH active site in competition with IMP or NAD^+ substrates.

Surprisingly, despite decades of intensive studies of IMPDHs, the role of their conserved Bateman domains remained unresolved at the molecular level. Our recent work has shown that they are involved in MgATP-dependent allosteric and oligomeric state regulations of bacterial IMPDHs [14, 15]. Only 3'-dATP and no other natural nucleotides were found to replace ATP, and full activation was obtained in the presence of a divalent cation, with Mn^{2+} ion being as efficient as Mg^{2+} ion [15]. Since then, GTP was shown to be a weak and natural negative effector of eukaryotic IMPDHs [16]. In addition, the binary complex formed by cyclophilin A and sanglifehrin A was recently shown to interact with the surface of the Bateman domain of the human IMPDH2 and to affect cell proliferation without affecting the enzymatic activity [17]. At the same time, Liao *et al.* [18] reported sappanone A, a homoisoflavonoid isolated from a plant, as a specific inhibitor of the human IMPDH2 by covalently binding to one cysteine residue within the Bateman domain. This compound has no effect on the human IMPDH1 as the cysteine residue (C140) is replaced by a serine residue, likewise in class 1 IMPDHs (**Fig. S5**). This compound was demonstrated in a mouse model to inhibit efficiently neuroinflammation, showing that targeting Bateman domain would be a way to develop therapeutic agents.

In this study, we screened a chemical library and identified the first-in-class allosteric inhibitors of the *Pseudomonas aeruginosa* IMPDH (designated herein as IMPDHpa). Twelve compounds were shown to be competitive for MgATP. Furthermore, our structural studies showed that these compounds bind into the Bateman domains by inducing a sharp but local rearrangement. In parallel, they maintain the protein in its overall apo form in marked contrast to the previously characterized holo form with the positive effector MnATP [15]. This study opens the road for the design of new series of bacterial inhibitors tightly binding to a so far orphan therapeutic target: bacterial IMPDHs.

2. Results

2.1. Selection of IMPDH inhibitors through screening of chemical libraries

The peculiar kinetic properties of class 1 IMPDHs [14, 15] suggest the possibility of developing specific allosteric inhibitors for these enzymes with a mode of action little explored so far. Indeed, these compounds will bind into the Bateman domain and compete for the positive effector (MgATP), unlike previously developed inhibitors, which bind into the core domain and are competitive with the natural substrates [10, 19]. To identify such inhibitors, a high-throughput screening of chemical libraries (total of 15,184 compounds) at an average concentration of 51.3 ± 10.5 µM (as the $K_{0.5}$ for IMP and the K_m for NAD are in the mM range) was performed on IMPDHpa (see flowchart **Fig. 1A**). IMPDHpa was selected as a representative of a class I IMPDHs as structural data were available for further characterization of the binding mode of the identified inhibitors. The libraries screened included structurally diverse synthetic compounds (either approved drugs, ATP mimics or nucleobase analogs). The assay based on NADH production monitored by optical absorbance at 340 nm (**Fig. S1B**) was done at non-saturating substrate concentrations (0.2 mM IMP, 0.4 mM NAD^+) and in the presence of ATP (0.2 mM) and $MgCl_2$ (3 mM). This condition will be considered as the reference (see Section 4.4 for details). Each 96-well plate was analyzed independently. First, using positive and negative controls, the value of the Z' factor [20] was determined (**Fig. S1A**). All values were above 0.5 (mean of 0.807 ± 0.073). Then the positive controls were used to calculate the slope value corresponding to 100 % catalytic activity and for each compound the % of inhibition was calculated. A hit was defined as a compound exhibiting more than 70% of inhibition of the catalytic activity (**Fig. S1C**) and led to the selection of twenty-five compounds (hit rate of 0.16 %; **Table S1**). Dose-response evaluations (**Fig. S1D**) were performed in the same assay conditions as for the screening: five

false positives and two compounds exhibiting half inhibitory concentration above 50 µM were eliminated, thus eighteen compounds were considered for further studies.

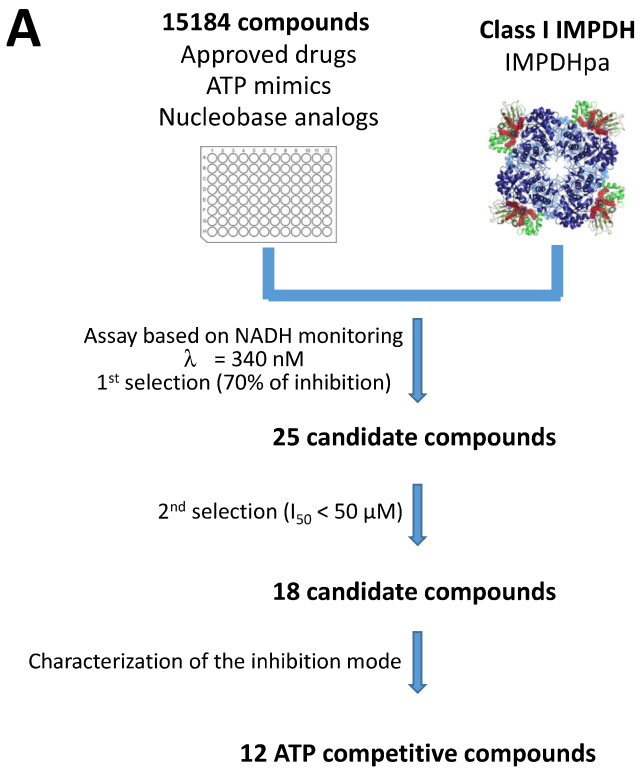

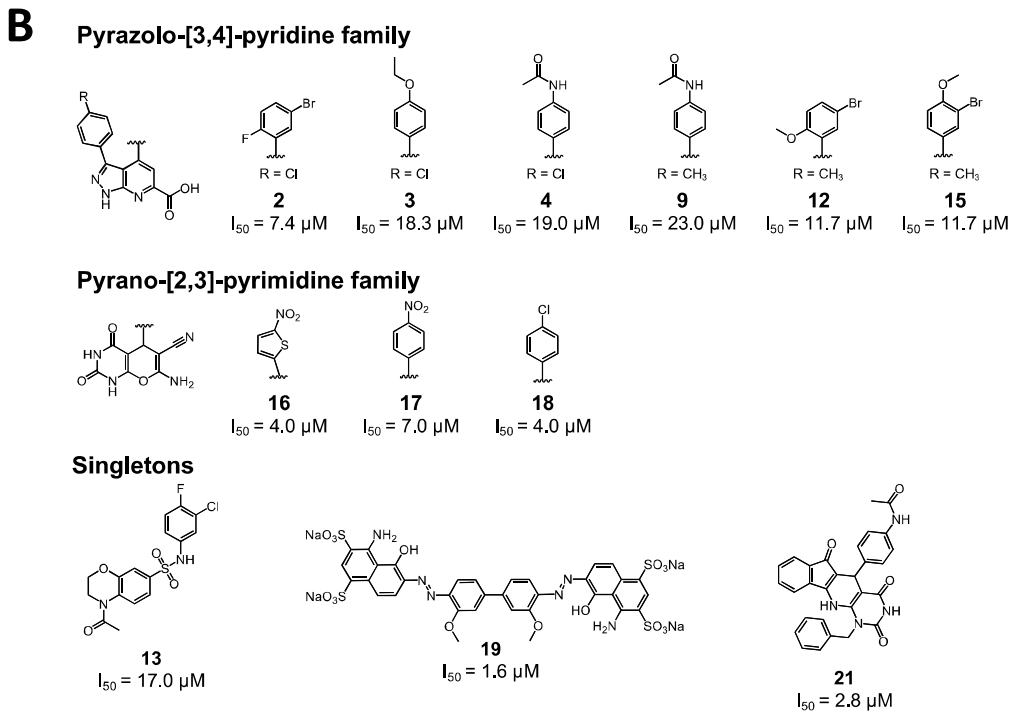

Figure 1: Screening strategy for identifying allosteric inhibitors. **A-** Overview showing the steps used to confirm and characterize compound hits starting from the primary screening. **B-** Structures of the 12 ATP competitive compounds classified by chemical scaffolds.

2.2. Insight into the inhibitory mechanism of the validated hits and identification of allosteric inhibitors

To decipher the mode of inhibition of the selected compounds, kinetic studies were performed using four different conditions: the reference condition (see above), and three other conditions, where the concentration of one component (either IMP, NAD^+ or ATP) was increased to 2 mM, whereas the others were kept the same as in the reference condition. For each condition, measurements were done in the presence or absence of the inhibitor at a concentration yielding 80% inhibition in the reference condition. Collectively, these data led to the identification of three types of inhibitors: five noncompetitive (for both substrates and ATP), one competitive for IMP and twelve competitive for ATP (**Table S1**). We have focused our attention on the third class of compounds, as only one chemical series has been

described as allosteric inhibitors for the human IMPDH2 (apart from the natural effectors such as ATP or GTP). These compounds (**Fig. 1B**) were clustered into two chemical families, namely pyrazolo-[3,4]-pyridine with six derivatives (**2**, **3**, **4**, **9**, **12** and **15**) and pyrano-[2,3]-pyrimidine with three derivatives (**16**, **17** and **18**), and three singletons (**13**, **19** and **21**). These compounds represent diverse set of compounds with unrelated chemical scaffolds. Compound **19**, as it is a well-known dye (i.e. Chicago sky blue 6B), was not considered for further studies.

At saturating concentration of NAD^+ (2 mM), the plot of IMPDHpa activity at variable concentrations of IMP was previously shown to be sigmoidal [15]. Addition of MgATP (0.2 mM) decreased the cooperativity index to almost 1 and the $K_{0.5}$ for IMP decreased by a factor of 3.4 (**Table 1**). The same experiment was conducted in the presence of a representative of each chemical series described above: **3**, **13**, **17** and **21** (**Fig. 1B**). In the presence of a fixed concentration of each compound (10 µM for **17** and **21** or 20 µM for **3** and **13**) and 0.2 mM MgATP, the kinetics were again best fitted with the Hill equation with n_H values varying from 1.2 (**17** and **21**) to 1.4 (**3** and **13**). The $K_{0.5}$ for IMP was also increased by a factor of 1.3-1.5 to 2.7. These results confirm that the compounds counteract the effect of the positive effector on IMPDHpa kinetic parameters.

To confirm the kinetic assay results, fluorescence experiments were performed. Previous studies have shown that IMPDHpa intrinsic fluorescence was not sensitive to the presence of MgATP [14]. We have thus investigated the fluorescence properties of a representative of each chemical series. One of them, namely compound **3** (see **Fig. 1B**), exhibits a fluorescence emission spectrum with a maximum at 470 nm upon excitation at 350 nm. Addition of IMPDHpa leads to a drastic change in the emission spectrum with an increase of the intensity and a blue shift of the maximum emission (**Fig. 2**). To verify the direct binding of compound **3** to the protein, size exclusion chromatography experiments on PD-10 desalting columns

(GE Healthcare) were performed with the compound alone or in the presence of IMPDHpa. The compound alone was stuck to the resin, and fluorescence signal was only detected when urea was added to the buffer. On the other hand, in the presence of IMPDHpa, fluorescence intensity corresponding to the compound was measured only in the fractions containing the protein. Altogether, these data clearly demonstrate the binding of this compound to IMPDHpa. For both experiments, the addition of MgATP totally or partially reversed the observed effects, i.e. shift of the fluorescence emission spectrum (see **Fig. 2**) and co-elution of the compound with IMPDHpa (data not shown). These results further support that the binding sites of the allosteric inhibitor and the positive effector (MgATP) are at least partially overlapping.

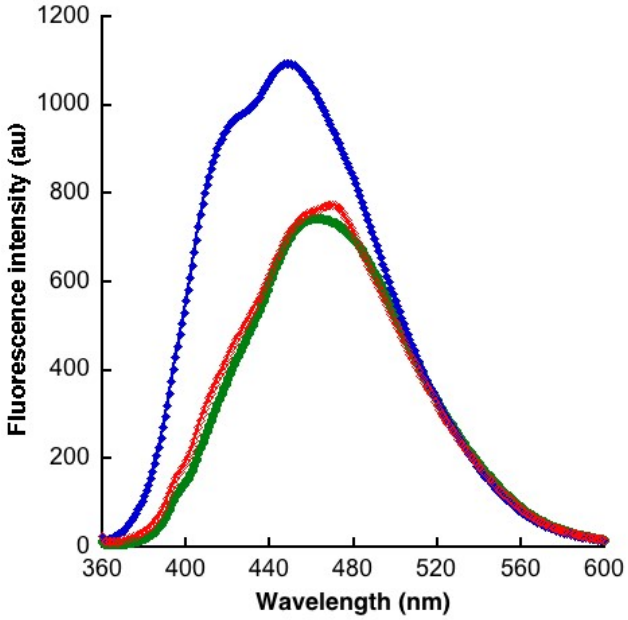

Figure 2: Compound **3** emission fluorescence spectra alone (1 µM, green), in the presence of 2 µM IMPDHpa without (blue) or with (red) 2 mM MgATP.

2.3. IMPDHpa structure of apo form and a complex with a pyrano-[2,3]-pyrimidine derivative.

SAXS experiments of IMPDHpa in the presence of an allosteric inhibitor representative of each chemical series (as an example **18**, **Fig. S2**) revealed that the inhibited protein has a similar shape to that of the apo enzyme, but markedly different from that in the presence of the positive effector. In order to confirm these results, we have undertaken the crystallization of the apo and inhibitor bound enzyme. New conditions were found using high throughput crystallization screening. Suitable crystals of IMPDHpa at 7.8 $mg.mL^{-1}$ could be grown in the presence of lithium chloride 500 mM, ammonium sulphate 50 mM and PEG8000 8% w/v) and high-resolution diffraction data (**Table 2**) were collected for both the apo form (2.11 Å) and the protein in complex with compound **18** at 50 μM (2.54 Å). The two structures were solved by molecular replacement using our previously solved structure of IMPDHpa (PDB4DQW [15]) as a starting template and further refined.

In both crystal structures, the asymmetric unit structures contain an octamer of IMPDHpa matching the expected octameric organization observed in solution [15] by means of SAXS and EM measurements (**Fig. S3**). Nevertheless, only six and five Bateman domains out of a total of eight are visible in the electron density of the apo and inhibited form, respectively (**Fig. 3A and 3B**). Contrary to our previous structure of IMPDHpa in the presence of the positive effector (**Fig. 3C**), the Bateman domains of the apo protein are more detached from the catalytic domain and the interface between the two tetramers, forming the octameric form, is decreased (with buried surfaces of 45,400 $Å^2$ for the ATP-bound state down to 33,610 A^2 for the apo-form and 36,130 $Å^2$ for the inhibited form). The protein is more flattened in the apo form than in the presence of MnATP with an axis shifted from 80 Å to 100 Å, respectively (see **Fig. 3A and 3C**, right panels).

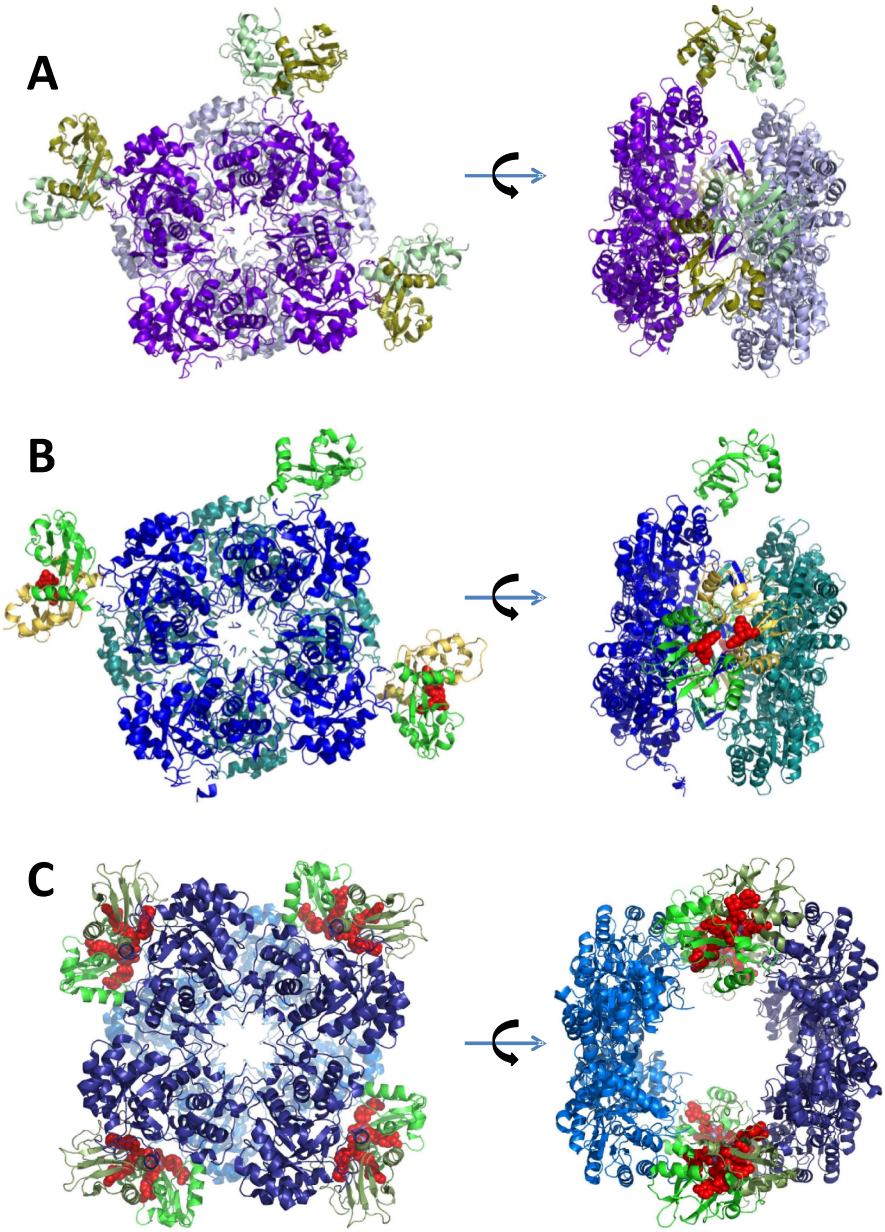

Figure 3: Comparison between the quaternary structures of IMPDHpa in its apo form (**A**), and in complex with the allosteric inhibitor **18** (**B**) or the positive effector, MnATP (**C**). Ribbon representations of IMPDHpa octamer viewed along the 4-fold axis (left panels) or perpendicular to it (right panels). The core domains of each tetramer are shown in a different color (blue or purple shades), as well as the Bateman domains (green shades). The allosteric inhibitor (compound **18**) and the positive effector (MnATP; PDB4DQW[15]) are shown as red spheres.

In agreement with previous studies of IMPDHpa and other IMPDHs, the active site in both structures is partially structured in the absence of either IMP or NAD. Indeed, the flap loop is not visible in the electron density maps and likely disordered. On the contrary, the finger loop forming the central octameric interface adopts a conformation already observed in the apo-form of the Bateman deletion mutant (PDB5AHL [21]) and other IMPDHs (PDB3FFS [22] and PDB1EEP [23]). In IMP-bound crystal structures, this loop is a bit tilted upon folding of the flap loop but it keeps a very similar conformation (in the presence or absence of ordered Bateman domains as well as in the IMP-bound Bateman-deletion mutants).

In parallel, the binding of the allosteric inhibitor induces an original rearrangement of the Bateman domains. Locally the structure differs from both the apo form (**Fig. 4A** and **4C**) and the MnATP-bound one (**Fig. 5A**), in agreement with the chemical dissimilarity of these positive and negative effectors. However, it partially involved the same region and the two binding sites partially overlap. Indeed, they both include residues Ile132, Arg136, Ile179 and Lys181 (**Fig. 4B**), all belonging to ATP binding cavity n°2 [15].

The pyrano-pyrimidine backbone of compound **18** is sandwiched with Ile179 and the phenyl group with Gly120, Ile132, Leu183 and Lys181 (**Fig. 4B** and **4D**). The carboxyl group of Val159 and Lys157 main chain interacts by hydrogen bonds with the nitrile and amine groups of compound **18**, respectively. Hydrogen bonds were also observed between nitrogen 1 and oxygen 4 atoms, and Arg136 from the opposite monomer and Lys181 residues, respectively. The involvement of residue of a second monomer constitutes the main difference between the binding sites of the allosteric inhibitor and the positive effector. A second variation comes from the number of binding sites, as there is only one allosteric inhibitor bound per Bateman domain whereas two positive effectors interact within one Bateman domain.

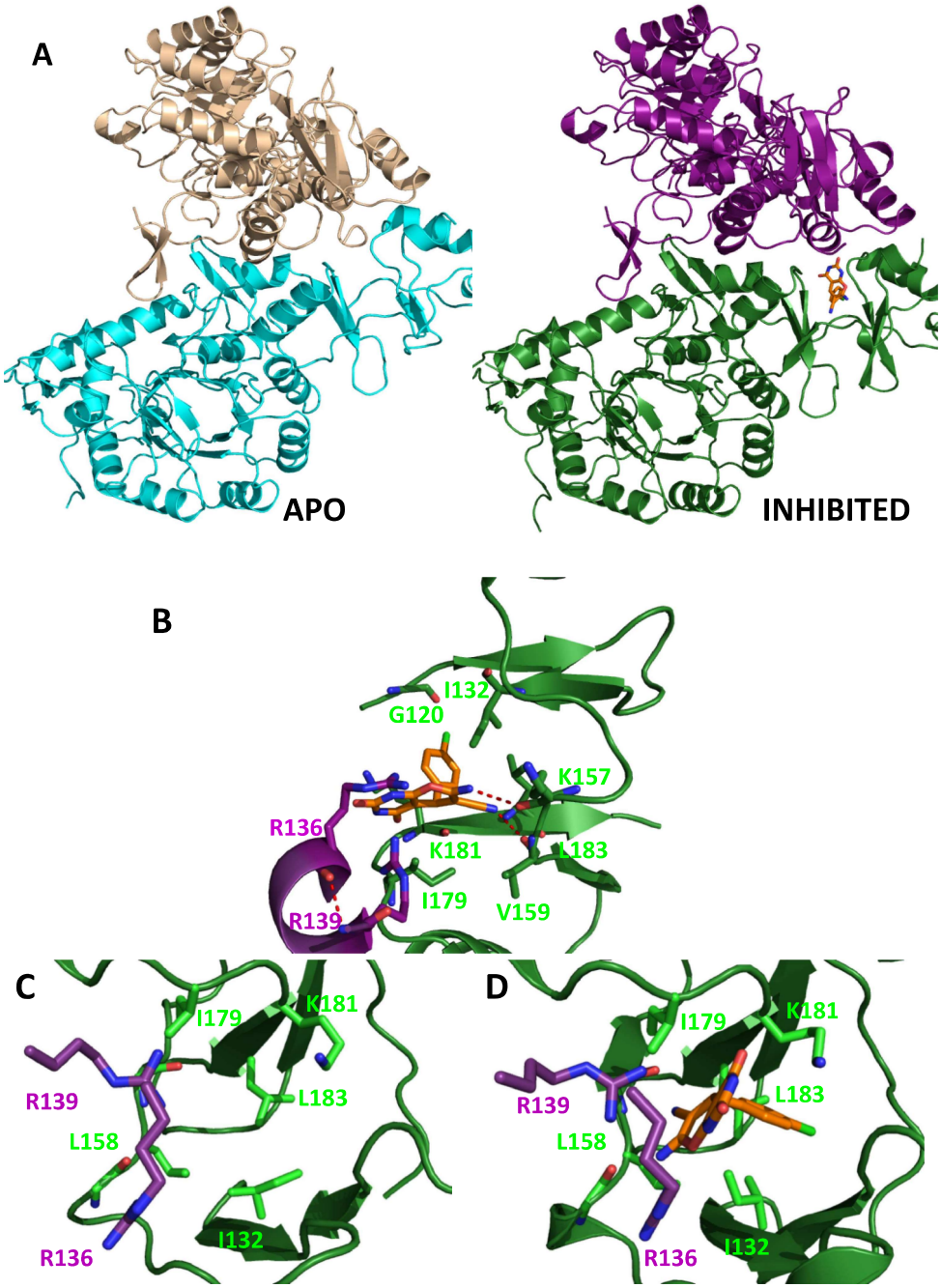

Figure 4: Structure of IMPDHpa with compound **18** and comparison with the apo structure. **A-** Ribbon representation of IMPDHpa monomers of apo form (left panel) and in complex with compound **18** (sticks; right panel). **B-** Detailed view of the allosteric inhibitor binding site within two adjacent Bateman domains (one monomer in green and the neighboring one in purple). The side chains of interacting residues and compound **18** (orange) are shown in sticks. The main hydrogen bounds are represented as red dashed lines. **C- and D-** Zoom on the allosteric binding pocket in the apo IMPDHpa and in the complex structures, respectively. Same color code as in B.

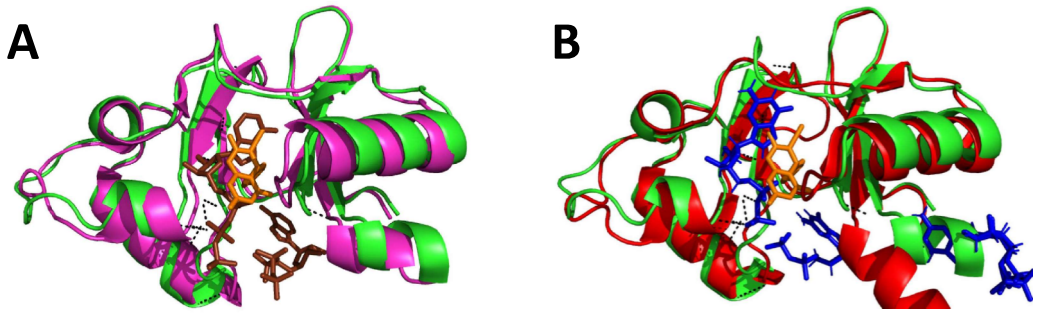

Figure 5: Overlay of the Bateman domains of IMPDHpa in complex with the allosteric inhibitor (green) and (**A**) the positive effector (pink) or (**B**) of IMPDHag in complex with GDP (red; PDB4Z87 [16]). The different molecules are represented as stick models: compound **18**, MnATP and GDP are colored in orange, brown and blue, respectively.

2.4. Ligand virtual docking

Taking advantage of the various crystal structures of IMPDHpa, we investigated the potential binding mode of the pyrazolo-[3,4]-pyridine and pyrano-[2,3]-pyrimidine families providing ATP-competitive inhibitors, as kinetic data of different derivatives were available for both chemical series (**Fig. 6**). Here, we used the ATP-bound state and the inhibited structure as templates for docking. The docking search was focus to the ligand binding pocket of the Bateman domain with boundaries defined using a distance threshold of 8 Å around the co-crystallized ligand. With (or without) their corresponding ligands (ATP and **18**) as shape restraints, similar poses were obtained for the two series in the Bateman domain in the inhibited form. Indeed, the three pyrano-[2,3]-pyrimidine derivatives (**16**, **17** and **18**) reproduce the binding mode observed in the crystal structure of the complex with **18**. Analysis using DSX-online [24] confirmed the quality of the docking poses with no major clashes and numerous favorable interactions (**Fig. S4**). The second series, which includes six pyrazolo-[3,4]-pyridine derivatives (**2**, **3**, **4**, **9**, **12** and **15**), was also docked satisfactorily,

with all these compounds oriented similarly in the adenine binding pocket. In this case, a similar binding mode was obtained in the ATP-bound conformation. The binding mode of **3** resembles partly that of the adenine moiety of the ATP molecule. Hence, the hydrophobic environment could explain the increase and blue-shifted fluorescence emission described above. These results suggested that these two series of micromolar hits can help the design of the first lead compounds to inhibit IMPDH through binding to the Bateman domains.

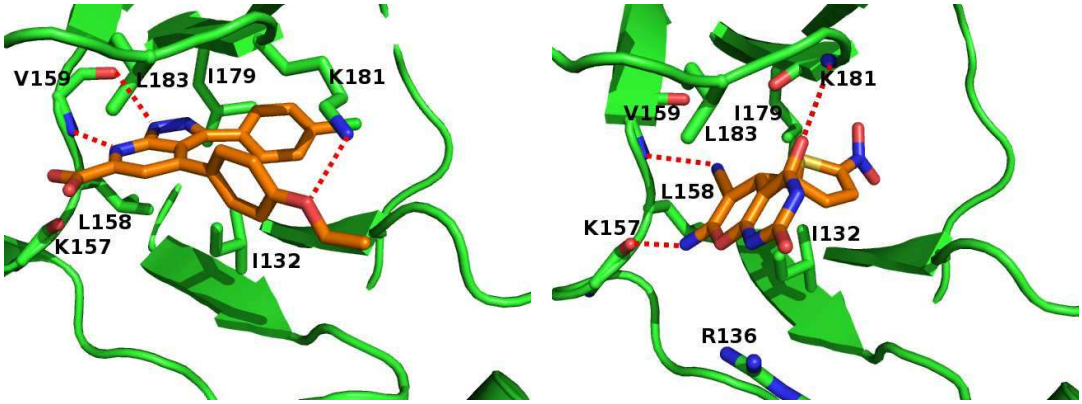

Figure 6: Predicted binding mode of compounds **3** (left panel) and **16** (right panel) with IMPDHpa. The two compounds and side-chain of interacting residues (mainly I132, V159, I179 and L183; see text) are shown as stick models. Hydrogen bonds are drawn as red dashed lines. The figure was drawn using Pymol (pymol.sourceforge.net).

3. Discussion

In this study, we have discovered new chemical series as allosteric inhibitors of class I IMPDHs. They were shown by complementary approaches to bind into the Bateman domain in the vicinity of the natural positive effector, and trap the protein in its apo form. Interestingly, the inhibitor-binding site is composed of residues from two adjacent monomers, with one binding site per monomer. On the other hand, there are two binding sites per Bateman domain involving residues from the same monomer for the natural positive effector (MgATP). Similarly, multiple binding pockets inside one single Bateman domain have been identified through structural studies of the eukaryotic *Ashbya gossypii* IMPDH [16] (IMPDHag). In this case, the three binding sites accommodate a natural negative effector, namely GDP. Nevertheless, superposition of the binding sites of the different inhibitors within the Bateman domains from IMPDHag and IMPDHpa (**Fig. 5B**) highlight that three ligands enter the same cleft but with distinct binding modes. The novel inhibitor binds in the cleft more deeply and induces a local rearrangement while the GDP in IMPDHag is mostly external at the entrance to the ATP binding site of IMPDHpa. These binding modes provide opportunities to guide new variations on these three compounds to derive better allosteric inhibitors. The plasticity/mobility of this domain, which is reflected by the fact that most of the time in crystal structures the Bateman domains are not visible, helps to explain the accommodation of diverse chemical compounds. On the other hand, the allosteric modulation of the catalytic activity seems to be conserved at the structural level between both IMPDHpa and IMPDHag and to involve large size variations. In line with our previous results [15, 21], the overall shape of the IMPDHpa octamer (**Fig. 7**) in complex with allosteric inhibitors or in the apo form (i.e. inhibitory form) is much more compact than the one in complex with MgATP (i.e. activated form). Crucial loops involved in the catalytic mechanism, such as the finger and C-terminal loops, which are ordered only in the apo form, interact in the inhibitory

form, leading to the rigidification of the core domain. The same scenario was seen with IMPDHag [25], with octamer compaction and finger interactions in the guanine nucleotides formed octamers (corresponding to the inhibitory form for this IMPDH), thus explaining the diminished catalytic efficiency of the enzyme in the presence of these guanine nucleotides.

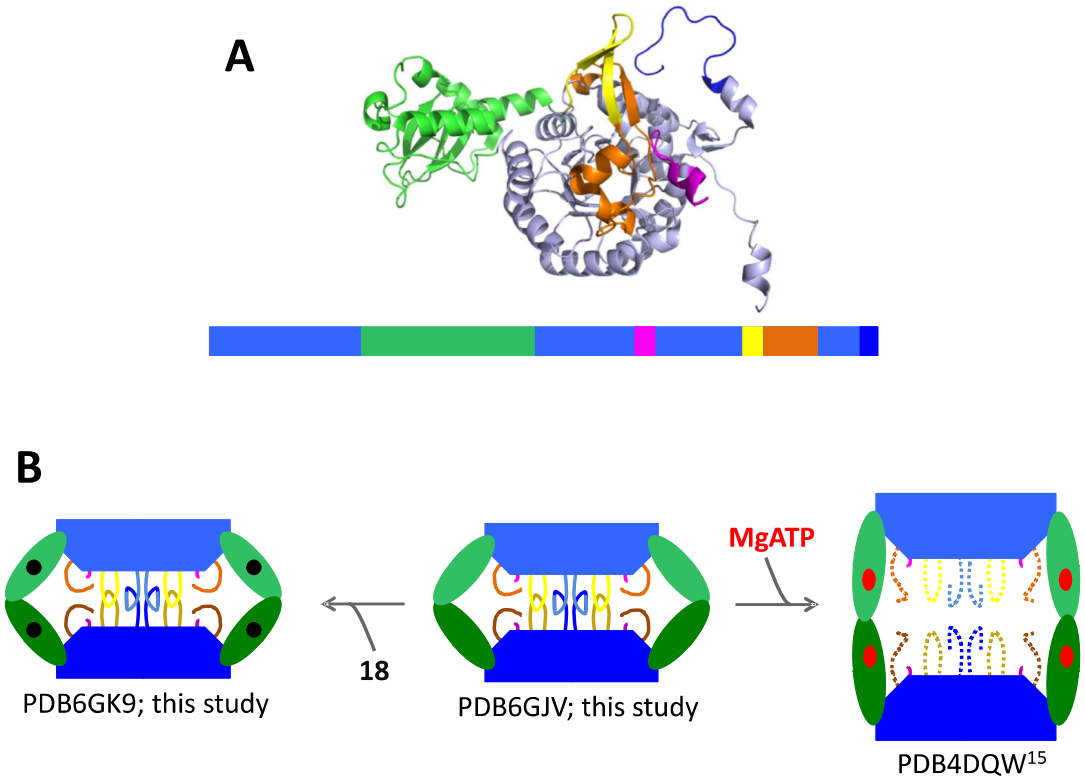

Figure 7: Proposed model of IMPDHpa quaternary structure modulation. **A-** IMPDHpa primary sequence as a schematic bar representation and X-ray structure of one monomer in ribbon representation. The Bateman domain and the core domain are colored in green and blue, respectively, as well as important loops of the core domain involved in the enzymatic activity: catalytic loop (residues 299–306, pink), flap loop (residues 384–421, orange), finger loop (residues 373–383, yellow) and C-terminal loop (residues 467–487, blue). **B-** Schematic representations of the apo and holo forms (in complex with MgATP or **18**). For each tetramer, the core domains are shown as a blue cone, and the Bateman domains or important loops are colored as in A. As all these loops are not ordered in the MgATP-bound form, they are represented as dashed lines. MgATP and **18** are shown as red circles and black squares, respectively.

In past years, IMPDH has been considered as a target for the development of novel antimicrobials [26]. *Cryptosporidum parvum* IMPDH (IMPDHcp) is of particular interest as this parasite lacks the enzymes required to salvage purine bases and thus is totally dependent on IMPDH for guanine nucleotides synthesis. A high-throughput screening was performed to identify inhibitors acting on the NAD site [27]. Several chemical series were identified and further developed such as benzoxazole derivatives [28]. Interestingly, this parasitic IMPDH is closely related to bacterial IMPDHs and some inhibitors of the IMPDHcp were found to be potent antibacterials [29, 30]. This has led to a renewed interest in bacterial IMPDHs [19]. Recent structural studies have revealed a NAD-binding pocket specific for bacterial IMPDHs [31], which could be exploited in the future for the development of more potent and selective inhibitors. Last year, starting from a phenotypic screen to search for novel anti-tubercular compounds, two different leads were found to target the *Mycobacterium tuberculosis* IMPDH, GuaB2 [32, 33]. In both cases, the binding sites were found to be located within the NAD binding pocket. Our recent data have provided new clues on the functional and structural role of the Bateman domain in IMPDH [14, 15]. We have thus chosen to target this regulatory domain instead of the core domain, which differs from the current approaches listed above, and could constitute another attractive way to develop novel antibacterial compounds. IMPDHpa Bateman domains are only 37% and 32% identical to the equivalent domains in human IMPDH 1 and IMPDH 2, respectively (see **Fig. S5**). This distant relationship should allow to derive specific binders due to several substitutions lining the binding site and directly contacting the current inhibitor (R139 versus D164, K157 versus D/E184, I179 versus K206 and L183 versus P210).

Looking into more detail into the IMPDHpa inhibitor binding site, no interaction between the chorine atom of the phenyl group of compound **18** and the protein was observed. This suggests that modulation of this chemical series might be possible with extensions from this

part of the molecule with the intent to increase the affinity of compound **18** for IMPDHpa and increase the inhibitory potency, as well as its solubility. Another possibility would be to take advantage of the adjacent binding site (**Fig. 4B**) and to link two pyrano-pyrimidine moieties with appropriate linkers.

4. Experimental section

4.1. Chemical libraries

The "Prestwick chemical library" (1,200 compounds) was purchased from Prestwick Chemical. The protein kinase targeted library (9,360 compounds) and the NECAN library (4,624 compounds) were acquired from ChemDiv. All compounds are in DMSO at a concentration of 2 mg/mL. NMR spectra of the 12 ATP competitive inhibitors (see **Fig 1B**) are provided in the Supplementary data (compound **19** from Prestwick Chemical, and the others from ChemDiv). Six of them were repurchased as powder (**3**, **13**, **15**, **17**, **18** and **21**).

4.2. Expression and purification of IMPDHpa

The expression and purification of IMPDHpa were performed as described previously [15]. Briefly, the recombinant protein expressed in *E. coli* was purified by affinity chromatography. For crystallization trials, a second step purification by size-exclusion chromatography was performed. IMPDHpa was stored in buffer A (20 mM potassium phosphate pH 8 and 25 mM KCl).

4.3. Activity assay of IMPDHpa

IMPDHpa activity was determined at 30 °C by monitoring the synthesis of NADH at 340 nm in an Eppendorf ECOM 6122 photometer (0.5 mL final volume). The reaction medium contained 50 mM Tris-HCl pH 8, 100 mM KCl, 1 mM DTT. Assays were performed at various concentrations of IMP, NAD^+, ATP, $MgCl_2$ and compounds identified herein, to which IMPDHpa (final concentration range: 0.1-3 µM) diluted in buffer A was added. One unit of enzyme activity corresponds to 1 µmole of product formed in 1 minute at 30°C at pH 8.

4.4. Chemical library screening

Screening was performed on a TECAN Freedom EVO® platform, measuring IMPDHpa

activity at 30°C by monitoring the synthesis of NADH. Compounds in DMSO were spiked from the mother plates in transparent, flat bottom, bar-coded 96-wells plates (columns 2 to 11). Columns 1 and 12 were positive and negative controls and were spiked with DMSO alone. Then, 100 µL of the reaction medium (50 mM Tris-HCl pH 8, 100 mM KCl, 1 mM DTT, 0.2 mM IMP, 0.4 mM NAD^+, 0.2 mM ATP and 2 mM $MgCl_2$) was added. After 2 min of incubation in a Peltier module at 30°C, the reaction was started by the addition of IMPDHpa (4.5 µg), except for the 8 negative controls where only buffer A (without IMPDHpa) was added. After 70 s shaking, absorbance at 340 nm was measured for 80 s (10 cycles, with 8 s interval) using a Sunrise (TECAN) plate reader thermostated at 37°C. For each well, the slope was calculated using a simple linear regression equation. For the compounds, data were expressed as % inhibition calculated as follows: % inhibition = (1 – (sample slope / mean of positive control slopes)) x 100.

4.5. Fluorescence spectroscopy

Measurements were performed on a FP-8200 spectrofluorimeter (Jasco) in a Peltier-thermostated cell holder, using a 10 mm path length quartz cell (Hellma). A bandwidth of 5 nm was used for the excitation and emission beams. The excitation wavelength was fixed at 350 nm and the emission spectra were recorded at 25°C, from 360 to 600 nm at a scan rate of 200 nm/min.

4.6. Solution X-ray diffusion

X-ray scattering was recorded on protein sample supplemented with the desired ligand on the SWING beamline at Synchrotron SOLEIL (Saclay, France) and processed as previously described [15].

4.7. Virtual screening

Ligand docking was performed on various crystal structures of IMPDHpa using the server @TOME-2[34] interfaced with PLANTS [35]. This combination allows parallel docking on

multiple conformations using automatic delimitations of binding site boundaries based on bound ligands. In addition, the same chemical entities can also be used to derive shape restraints.

4.8. Crystallization and X-ray diffraction data collection

Initial screening of crystallization conditions was carried out by the vapour diffusion method using a MosquitoTM nanoliter-dispensing system (TTP Labtech). Sitting drops were set up using 400 nL of a 1:1 mixture of each sample protein and crystallization solutions (672 different commercially available conditions) equilibrated against a 150 µL reservoir in multiwell plates (Greiner Bio-One). The crystallization plates were stored at 18°C in a RockImager1000® (Formulatrix) automated imaging system to monitor crystal growth. Crystallization hits were improved using manually prepared hanging drops in 24-well plates at the same temperature.

Optimized conditions for crystal growth were as follows: the best crystals (in apo form and in the presence of compound **18** at 50 µM) were obtained by mixing 1.5 µL of protein at 7.8 $mg.mL^{-1}$ (in buffer B) with 1.5 µL reservoir solution containing 500 mM of lithium chloride, 50 mM of ammonium sulfate, and 8% of PEG8000.

Single crystals of the IMPDHpa in its apo form and in complex with compound **18** were flash-cooled in liquid nitrogen using a mixture of 70 % crystallization solution and 30 % ethylene glycol as cryoprotectant.

All X-ray diffraction data were collected on beamline PROXIMA-1 at synchrotron SOLEIL (St Aubin, France). Diffraction images were integrated with the program XDS[36] and crystallographic calculations were carried out with programs from the CCP4 program suite[37]. Molecular replacement was done using Molrep [38]. Rigid body and restrained refinement was done using Refmac5 [39], with alternating manual rebuilding in Coot[40].

The refined models and structure factors have been deposited in the Research Collaboration

for Structural Biology Protein Data Bank (hyperlink "http://www.rcsb.org/") under the following accession numbers: PDB6GJV (IMPDHpa apo form) and PDB6GK9 (IMPDHpa/**18**).

Acknowledgements

We thank Emilie Dufour for participation in the chemical library screening, Zakaria Jemouai for participation in the kinetic characterization of the allosteric inhibitors and Aurélie Bourderioux for performing the fluorescence experiments. We thank the Molecular Biophysics facility (PFBMI, Institut Pasteur, Paris) for their technical assistance and helpful suggestions. The authors are grateful to the staff of the Crystallographic platform from the Institut Pasteur for robot-driven crystallization screening. We thank Alexandre Chenal for fruitful discussion and technical assistance for fluorescence experiments, and Thomas J. Dougherty for careful reading of this manuscript.

We acknowledge the Synchrotron SOLEIL (St Aubin, France) staff for assistance and advice during data collection on PROXIMA-1 (X-ray diffraction data) and SWING (SAXS data) beamlines.

Funding sources

This work was supported in part by the Centre National de la Recherche Scientifique (CNRS), the Institut National de la Santé Et de la Recherche Médicale (INSERM), the Institut Pasteur, the Conseil Régional d'Ile-de-France (Chemical Library Project, grants n° I 06-222/R and I 09-1739/ R, which included a postdoctoral fellowship for Alexandru Lupan) and the French Infrastructure for Integrated Structural Biology (FRISBI) ANR-10-INBS-05.

Thomas Alexandre was a recipient of a PhD fellowship from the Conseil Régional d'Ile-de-France and the "D.I.M. maladies infectieuses, parasitaires et nosocomiales émergentes" 2011.

Conflicts of interest

The authors declare no competing financial interest.

Supplementary data

Supplementary data include one table, five figures and NMR spectra.

References

[1] A. Bateman, The structure of a domain common to archaebacteria and the homocystinuria disease protein, Trends Biochem. Sci., 22 (1997) 12-13.
[2] M.D. Sintchak, M.A. Fleming, O. Futer, S.A. Raybuck, S.P. Chambers, P.R. Caron, M.A. Murcko, K.P. Wilson, Structure and Mechanism of Inosine Monophosphate Dehydrogenase in Complex with the Immunosuppressant Mycophenolic Acid, Cell, 85 (1996) 921-930.
[3] J. Ereño-Orbea, I. Oyenarte, L.A. Martinez-Cruz, CBS domains: Ligand binding sites and conformational variability, Arch.Biochem. Biophys., 540 (2013) 70-81.
[4] S. Ignoul, J. Eggermont, CBS domains: structure, function, and pathology in human proteins, Am. J. Physiol. Cell Physiol., 289 (2005) C1369-C1378.
[5] J.W. Scott, S.A. Hawley, K.A. Green, M. Anis, G. Stewart, G.A. Scullion, D.G. Norman, D.G. Hardie, CBS domains form energy-sensing modules whose binding of adenosine ligands is disrupted by disease mutations, J. Clin. Invest., 113 (2004) 274-284.
[6] J. Ereño-Orbea, T. Majtan, I. Oyenarte, J.P. Kraus, L.A. Martínez-Cruz, Structural basis of regulation and oligomerization of human cystathionine β-synthase, the central enzyme of transsulfuration, Proc. Natl. Acad. Sci. USA, 110 (2013) E3790-E3799.
[7] A.L. Pey, T. Majtan, J.M. Sanchez-Ruiz, J.P. Kraus, Human cystathionine β-synthase (CBS) contains two classes of binding sites for S-adenosylmethionine (SAM): complex regulation of CBS activity and stability by SAM, Biochemical Journal, 449 (2013) 109-121.
[8] D.G. Hardie, F.A. Ross, S.A. Hawley, AMPK: a nutrient and energy sensor that maintains energy homeostasis, Nat. Rev. Mol. Cell Biol., 13 (2012) 251-262.
[9] A. Accardi, Structure and gating of CLC channels and exchangers, J. Physiol., 593 (2015) 4129-4138.
[10] L. Hedstrom, IMP dehydrogenase: structure, mechanism, and inhibition, Chem. Rev., 109 (2009) 2903-2928.
[11] Q. Shu, V. Nair, Inosine monophosphate dehydrogenase (IMPDH) as a target in drug discovery, Med. Res. Rev., 28 (2008) 219-232.
[12] R. Bentley, Mycophenolic Acid: A One Hundred Year Odyssey from Antibiotic to Immunosuppressant, Chemical Reviews, 100 (2000) 3801-3826.
[13] L. Chen, K.W. Pankiewicz, Recent development of IMP dehydrogenase inhibitors for the treatment of cancer, Curr. Opin. Drug Discov. Devel., 10 (2007) 403-412.
[14] T. Alexandre, B. Raynal, H. Munier-Lehmann, Two classes of bacterial IMPDHs according to their quaternary structures and catalytic properties, PLoS ONE, 10 (2015) e0116578.
[15] G. Labesse, T. Alexandre, L. Vaupré, I. Salard-Arnaud, J.L.K. Him, B. Raynal, P. Bron, H. Munier-Lehmann, MgATP Regulates Allostery and Fiber Formation in IMPDHs, Structure, 21 (2013) 975-985.
[16] R.M. Buey, R. Ledesma-Amaro, A. Velazquez-Campoy, M. Balsera, M. Chagoyen, J.M. de Pereda, J.L. Revuelta, Guanine nucleotide binding to the Bateman domain mediates the allosteric inhibition of eukaryotic IMP dehydrogenases, Nat Commun, 6 (2015) 8923.
[17] K.H. Pua, D.T. Stiles, M.E. Sowa, G.L. Verdine, IMPDH2 Is an Intracellular Target of the Cyclophilin A and Sanglifehrin A Complex, Cell Rep, 18 (2017) 432-442.

[18] L.X. Liao, X.M. Song, L.C. Wang, H.N. Lv, J.F. Chen, D. Liu, G. Fu, M.B. Zhao, Y. Jiang, K.W. Zeng, P.F. Tu, Highly selective inhibition of IMPDH2 provides the basis of antineuroinflammation therapy, Proc Natl Acad Sci U S A, 114 (2017) E5986-E5994.
[19] L. Hedstrom, G. Liechti, J.B. Goldberg, D.R. Gollapalli, The antibiotic potential of prokaryotic IMP dehydrogenase inhibitors, Curr. Med. Chem., 18 (2011) 1909-1918.
[20] J.H. Zhang, T.D. Chung, K.R. Oldenburg, A Simple Statistical Parameter for Use in Evaluation and Validation of High Throughput Screening Assays, J. Biomol. Screening, 4 (1999) 67-73.
[21] G. Labesse, T. Alexandre, M. Gelin, A. Haouz, H. Munier-Lehmann, Crystallographic studies of two variants of *Pseudomonas aeruginosa* IMPDH with impaired allosteric regulation, Acta Crystallographica Section D, 71 (2015) 1890-1899.
[22] I.S. Macpherson, S. Kirubakaran, S.K. Gorla, T.V. Riera, J.A. D'Aquino, M. Zhang, G.D. Cuny, L. Hedstrom, The structural basis of *Cryptosporidium*-specific IMP dehydrogenase inhibitor selectivity, J. Am. Chem. Soc., 132 (2010) 1230-1231.
[23] F.M. McMillan, M. Cahoon, A. White, L. Hedstrom, G.A. Petsko, D. Ringe, Crystal structure at 2.4 A resolution of *Borrelia burgdorferi* inosine 5'-monophosphate dehydrogenase: evidence of a substrate-induced hinged-lid motion by loop 6, Biochemistry, 39 (2000) 4533-4542.
[24] H. Gohlke, M. Hendlich, G. Klebe, Knowledge-based scoring function to predict protein-ligand interactions, J Mol Biol, 295 (2000) 337-356.
[25] R.M. Buey, D. Fernandez-Justel, I. Marcos-Alcalde, G. Winter, P. Gomez-Puertas, J.M. de Pereda, J. Luis Revuelta, A nucleotide-controlled conformational switch modulates the activity of eukaryotic IMP dehydrogenases, Sci Rep, 7 (2017) 2648.
[26] C.P. Shah, P.S. Kharkar, Inosine 5′ -monophosphate dehydrogenase inhibitors as antimicrobial agents: recent progress and future perspectives, Future Medicinal Chemistry, 7 (2015) 1415-1429.
[27] N.N. Umejiego, D. Gollapalli, L. Sharling, A. Volftsun, J. Lu, N.N. Benjamin, A.H. Stroupe, T.V. Riera, B. Striepen, L. Hedstrom, Targeting a prokaryotic protein in a eukaryotic pathogen: identification of lead compounds against cryptosporidiosis, Chem. Biol., 15 (2008) 70-77.
[28] S.K. Gorla, M. Kavitha, M. Zhang, J.E. Chin, X. Liu, B. Striepen, M. Makowska-Grzyska, Y. Kim, A. Joachimiak, L. Hedstrom, G.D. Cuny, Optimization of Benzoxazole-Based Inhibitors of *Cryptosporidium parvum* Inosine 5′ -Monophosphate Dehydrogenase, J. Med. Chem., 56 (2013) 4028-4043.
[29] D.R. Gollapalli, I.S. Macpherson, G. Liechti, S.K. Gorla, J.B. Goldberg, L. Hedstrom, Structural determinants of inhibitor selectivity in prokaryotic IMP dehydrogenases, Chem Biol, 17 (2010) 1084-1091.
[30] K. Mandapati, S.K. Gorla, A.L. House, E.S. McKenney, M. Zhang, S.N. Rao, D.R. Gollapalli, B.J. Mann, J.B. Goldberg, G.D. Cuny, I.J. Glomski, L. Hedstrom, Repurposing Cryptosporidium Inosine 5′ -Monophosphate Dehydrogenase Inhibitors as Potential Antibacterial Agents, ACS Medicinal Chemistry Letters, 5 (2014) 846-850.
[31] M. Makowska-Grzyska, Y. Kim, N. Maltseva, J. Osipiuk, M. Gu, M. Zhang, K. Mandapati, D.R. Gollapalli, S.K. Gorla, L. Hedstrom, A. Joachimiak, A Novel Cofactor-binding Mode in Bacterial IMP Dehydrogenases Explains Inhibitor Selectivity, J. Biol. Chem., 290 (2015) 5893-5911.
[32] Y. Park, A. Pacitto, T. Bayliss, L.A. Cleghorn, Z. Wang, T. Hartman, K. Arora, T.R. Ioerger, J. Sacchettini, M. Rizzi, S. Donini, T.L. Blundell, D.B. Ascher, K. Rhee, A. Breda, N. Zhou, V. Dartois, S.R. Jonnala, L.E. Via, V. Mizrahi, O. Epemolu, L. Stojanovski, F. Simeons, M. Osuna-Cabello, L. Ellis, C.J. MacKenzie, A.R. Smith, S.H. Davis, D. Murugesan, K.I.

Buchanan, P.A. Turner, M. Huggett, F. Zuccotto, M.J. Rebollo-Lopez, M.J. Lafuente-Monasterio, O. Sanz, G.S. Diaz, J. Lelievre, L. Ballell, C. Selenski, M. Axtman, S. Ghidelli-Disse, H. Pflaumer, M. Bosche, G. Drewes, G.M. Freiberg, M.D. Kurnick, M. Srikumaran, D.J. Kempf, S.R. Green, P.C. Ray, K. Read, P. Wyatt, C.E. Barry, 3rd, H.I. Boshoff, Essential but Not Vulnerable: Indazole Sulfonamides Targeting Inosine Monophosphate Dehydrogenase as Potential Leads against Mycobacterium tuberculosis, ACS Infect Dis, 3 (2017) 18-33.
[33] V. Singh, S. Donini, A. Pacitto, C. Sala, R.C. Hartkoorn, N. Dhar, G. Keri, D.B. Ascher, G. Mondesert, A. Vocat, A. Lupien, R. Sommer, H. Vermet, S. Lagrange, J. Buechler, D.F. Warner, J.D. McKinney, J. Pato, S.T. Cole, T.L. Blundell, M. Rizzi, V. Mizrahi, The Inosine Monophosphate Dehydrogenase, GuaB2, Is a Vulnerable New Bactericidal Drug Target for Tuberculosis, ACS Infect Dis, 3 (2017) 5-17.
[34] J.L. Pons, G. Labesse, @TOME-2: a new pipeline for comparative modeling of protein-ligand complexes, Nucleic Acids Res., 37 (2009) W485-491.
[35] O. Korb, T. Stützle, T.E. Exner, An ant colony optimization approach to flexible protein–ligand docking, Swarm Intell, 1 (2007) 115-134.
[36] W. Kabsch, Xds, Acta Crystallogr D Biol Crystallogr, 66 (2010) 125-132.
[37] M.D. Winn, C.C. Ballard, K.D. Cowtan, E.J. Dodson, P. Emsley, P.R. Evans, R.M. Keegan, E.B. Krissinel, A.G. Leslie, A. McCoy, S.J. McNicholas, G.N. Murshudov, N.S. Pannu, E.A. Potterton, H.R. Powell, R.J. Read, A. Vagin, K.S. Wilson, Overview of the CCP4 suite and current developments, Acta Crystallogr D Biol Crystallogr, 67 (2011) 235-242.
[38] A. Vagin, A. Teplyakov, Molecular replacement with MOLREP, Acta Crystallogr. D Biol. Crystallogr., 66 (2010) 22-25.
[39] G.N. Murshudov, A.A. Vagin, E.J. Dodson, Refinement of macromolecular structures by the maximum-likelihood method, Acta Crystallogr. D Biol. Crystallogr., 53 (1997) 240-255.
[40] P. Emsley, K. Cowtan, Coot: model-building tools for molecular graphics, Acta Crystallogr. D Biol. Crystallogr., 60 (2004) 2126-2132.